

# Speeding up a few orders of magnitude the Jacobi method: high order Chebyshev-Jacobi over GPUs

J.E. Adsuara<sup>a,\*</sup>, M.A. Aloy<sup>a,\*</sup>, P. Cerdá-Durán<sup>a,\*</sup>, I. Cordero-Carrión<sup>b,\*</sup>

<sup>a</sup>*Departamento de Astronomía y Astrofísica, Universidad de Valencia, E-46100, Burjassot, Spain.*

<sup>b</sup>*Departamento de Matemáticas, Universidad de Valencia, E-46100, Burjassot, Spain.*

---

## Abstract

In this technical note we show how to reach a remarkable speed up when solving elliptic partial differential equations with finite differences thanks to the joint use of the Chebyshev-Jacobi method with high order discretizations and its parallel implementation over GPUs.

*Keywords:* Iterative methods, Jacobi, Scheduled Relaxation Jacobi, Chebyshev-Jacobi, Finite difference, Elliptic equations, Parallelism, GPUs.

---

## 1. Introduction

In [1, 2, 3] a generalization of the weighted Jacobi method for linear systems was presented and improved. Adsuara et al. [4] showed that this new Chebyshev-Jacobi method (CJM) is equivalent to a Generalized Richardson iterative scheme. These authors showed how to obtain analytically the weights not only for the classical 5-points discretization of the Laplacian operator, but also for high order discretizations, involving a larger number of points. They found that using higher-order discretizations of the Laplacian is always advantageous, since they lead to a solution of the same quality than lower-order discretizations, but in a shorter time. This point in combination with the trivial parallelization of the method predicts a promising performance. Here, we go an step forward by parallelizing the CJM for GPUs.

This note is organized as follows. In Section 2 we recap the essentials of the CJM with high-order discretizations and the methodological steps to

---

\*jose.adsuara@uv.es, miguel.a.aloy@uv.es, pablo.cerda@uv.es, isabel.cordero@uv.es

port it to the GPU technology. In Section 3 we show the speed up of the new implementation in various GPU architectures. Finally, in the last section, we summarize the main achievements of the article and define the outlines for the future work.

## 2. Methodology

In the following subsections we first present a brief summary of the CJM and then comment on the various ingredients involved in our analysis of the acceleration factors for the different GPU architectures.

### *2.1. The CJM with a high order discretization of the Laplacian*

As showed in [4], the CJM is the optimal one of all the possible schemes introduced previously in [1, 2, 3]. Briefly, the CJM consists on a weighted classical Jacobi method with strictly different weights at each iteration. A particular scheme is defined then by a set of weights, which is precalculated before starting the iterative algorithm as a transformation of the zeros of a Chebyshev polynomial. This transformation depends, among other aspects, on the resolution of the mesh, the boundary conditions and the required tolerance. The grid resolution and boundary conditions determine the wave numbers of elementary trigonometric waves that one can fit on the mesh. This allow us to bound the eigenvalues of the iteration matrix to the interval  $[\kappa_{\min}, \kappa_{\max}]$ , whose boundaries can be obtained analytically (see below).

When finite differences are used in order to solve elliptic partial differential equations, the problem reduces to solving a linear system. A CJM can be used and the corresponding transformation of the zeros of a Chebyshev polynomial also depends on the resulting matrix associated to the linear system. As it has been already mentioned in [4], the classical 5-points discretization of the bidimensional Laplacian leads to a consistently ordered (CO) matrix, where Young's theory is applicable. However, there are many other useful discretizations [5], which end up with a non-consistently ordered matrix, where Young's theory cannot be used.

In [4] we presented two parametrized discretizations of the Laplacian in two spatial dimensions, which can achieve an order of accuracy larger than two. In this note we use one discretization of each of these two families. From the first family, we use a 9-point discretization corresponding to a value of

the parameter in [4] of  $\alpha = \frac{2}{3}$ , whose Laplacian is discretized as

$$\begin{aligned} \Delta u_{ij} = \frac{1}{6h^2} & \left[ 4u_{i-1,j} + 4u_{i+1,j} + 4u_{i,j-1} + 4u_{i,j+1} \right. \\ & \left. + u_{i-1,j-1} + u_{i+1,j+1} + u_{i-1,j+1} + u_{i+1,j-1} - 20u_{i,j} \right] \end{aligned} \quad (1)$$

and whose  $\kappa_{\min}$  and  $\kappa_{\max}$  values, needed for obtaining the scheme and related with the size of the mesh, are

$$\kappa_{\min}^{(9)} = \frac{4}{5} \left[ \sin^2 \frac{\pi}{2N_x} + \sin^2 \frac{\pi}{2N_y} \right] \quad (2)$$

$$+ \frac{1}{5} \left[ \sin^2 \left( \frac{\pi}{2N_x} + \frac{\pi}{2N_y} \right) + \sin^2 \left( \frac{\pi}{2N_x} - \frac{\pi}{2N_y} \right) \right], \quad (3)$$

$$\kappa_{\max}^{(9)} = \frac{8}{5}, \quad (4)$$

where the subscript (9) refers to the number of points in which the Laplacian operator is discretized, and  $N_x$  and  $N_y$  are the number of points per dimension in the spatial directions  $x$  and  $y$ , respectively. The grid assumed in this discretization is uniform, so that  $L_x/N_x = L_y/N_y := h$ ,  $L_x$  and  $L_y$  being the sizes along the  $x$ - and  $y$ - directions, respectively.

From the second family of discretizations, we use a 17-point discretization with  $\alpha = \frac{2}{3}$ , whose discrete representation of the Laplacian reads

$$\begin{aligned} \Delta u_{ij} = \frac{1}{72h^2} & \left[ -4u_{i-2,j} + 64u_{i-1,j} + 64u_{i+1,j} - 4u_{i+2,j} \right. \\ & -4u_{i,j-2} + 64u_{i,j-1} + 64u_{i,j+1} - 4u_{i,j+2} \\ & -u_{i-2,j-2} + 16u_{i-1,j-1} + 16u_{i+1,j+1} - u_{i+2,j+2} \\ & \left. -u_{i-2,j+2} + 16u_{i-1,j+1} + 16u_{i+1,j-1} - u_{i+2,j-2} - 300u_{i,j} \right]. \end{aligned} \quad (5)$$

and whose corresponding  $\kappa_{\min}$  and  $\kappa_{\max}$  values are

$$\begin{aligned} \kappa_{\min}^{(17)} = & -\frac{4}{75} \left[ \sin^2 \frac{\pi}{N_x} + \sin^2 \frac{\pi}{N_y} \right] + \frac{64}{75} \left[ \sin^2 \frac{\pi}{2N_x} + \sin^2 \frac{\pi}{2N_y} \right] \\ & - \frac{1}{75} \left[ \sin^2 \left( \frac{\pi}{N_x} + \frac{\pi}{N_y} \right) + \sin^2 \left( \frac{\pi}{N_x} - \frac{\pi}{N_y} \right) \right] \end{aligned} \quad (6)$$

$$+ \frac{16}{75} \left[ \sin^2 \left( \frac{\pi}{2N_x} + \frac{\pi}{2N_y} \right) + \sin^2 \left( \frac{\pi}{2N_x} - \frac{\pi}{2N_y} \right) \right] \quad (7)$$

$$\kappa_{\max}^{(17)} = \frac{128}{75}. \quad (8)$$

In Figure 1 we show a schematic view of the two stencils for the two different discretizations along with the numerical coefficients corresponding to each node. Note that the value of the discrete Laplacian operator evaluated at the central node is a weighted sum over all the nodes schematically represented in each of the figure panels. The purpose of these schemes is showing that given a central point, the Laplacian discretization is fully specified by providing a list of  $M$  numerical coefficients enclosed in all the surrounding nodes.

## 2.2. GPUs

Modern GPUs have become extremely powerful processing units, which can accelerate enormously the computation of heavy mathematical operations. However, for that to happen, the algorithms must be properly vectorized and the pipeline of arithmetic operations and data transfers from/to the main memory must be optimized. The CJM method is perfectly suited for its porting to GPUs. In each iteration of the method the approximate solution is stored in each node and we must apply the same set of elementary arithmetic operations to each of them.

## 3. Results

In this section we show the execution times obtained when solving a particular problem in the two discretizations introduced above using two specific GPUs models.

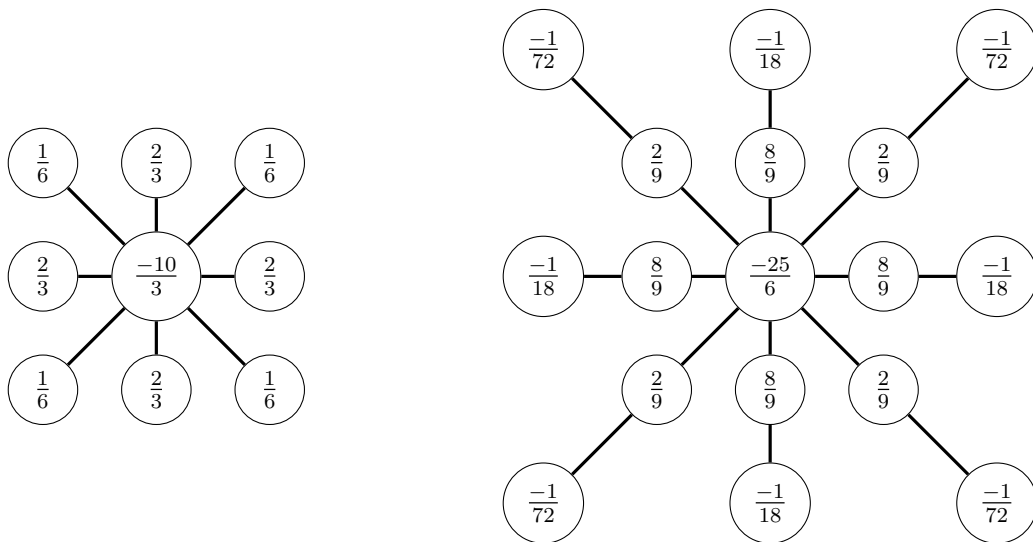


**Figure 1:** Schematic representation of the 9-points and 17-point discretizations of the Laplacian in two spatial dimensions, corresponding to a value  $\alpha = \frac{2}{3}$ . Each circle corresponds to a neighboring point of a given one  $(i, j)$ , represented by the central circle. The value enclosed by each circumference corresponds to the coefficient of the discretizations shown in Eqs. 1 and 5 multiplied by  $h^2$ . See [4] for details.

### 3.1. CUDA devices

We present in this subsection the specific devices we used. We aim to test more than a single GPU model in order to properly assess the scaling properties of our implementation of the CJM, which is based on the CUDA [6] technology of NVIDIA. CUDA devices can be characterized by two parameters (among others): the Compute Capability (CC) and the number of Streaming Multiprocessors (SMs). The CC of a device is represented by a version number. It comprises a major revision number  $X$  and a minor revision number  $Y$ , and it is denoted with the format “ $X.Y$ ”. Devices with the same major revision number belong to the same core architecture.

We have used two CUDA devices: a Tesla K40c and a GeForce GTX Titan X, with CC values of 3.5 and 5.2, respectively. We note that the major revision numbers are different. They correspond to two distinct architectures, Kepler and Maxwell, with major revision numbers 3 and 5, respectively. These GPU devices are connected to two different computers, having CPUs Dual-Core AMD Opteron 2222 working at a frequency of 3 GHz and Intel 7-4820K with a working frequency of 3.70 GHz, respectively. We will refer to the CPUs of these systems as Kp and Mw, respectively. In our first device we have 15 SMs, while in the second one we have 24 SMs. We have decided to use both types of hardware because, although the Maxwell microarchitecture is more recent and, a priori, better in many technical aspects, it seems that double precision arithmetics (required for practical applications of the CJM) works better on Kepler than on Maxwell. Table 1 summarizes the relevant properties of the two architectures employed in this paper.

CPU	Device	Architecture	CC	SMs
Opteron (Kp)	Tesla K40c	Kepler	3.5	15
Intel (Mx)	GeForce GTX Titan X	Maxwell	5.2	24

**Table 1:** Properties of the two GPU architectures in which the CJM has been tested. We note that the memory on board (12 Gb) is the same for both GPUs.

### 3.2. Code

In order to execute the Jacobi method and the CJM over GPUs, we have developed two CUDA kernels, i.e., sections of code that instead of running on the CPU run on the GPU device. We need to transfer the data that the kernel will use from the memory of the host to that of the device. Once the

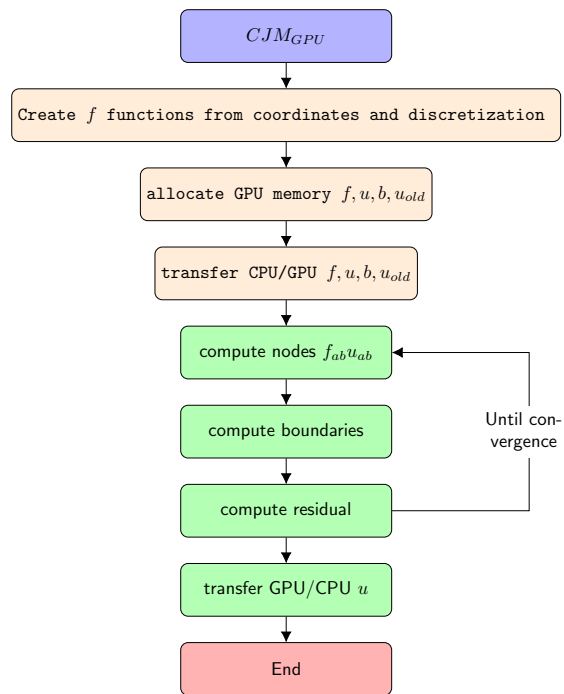


**Figure 2:** Flow chart of the code.  $b$  stands for the source term (if any) of the elliptic partial differential equation. Green background rectangles correspond to execution blocks in the GPU device. The rest of the execution blocks take place on the host computer.

results are computed, they are transferred back from the device to the host. The 12GB of memory of our devices is large enough to allow us to transfer the whole data structure of the problem to the GPU memory in one transfer at the beginning of the calculation. Once the problem has been solved to the desired accuracy (fully on the GPU device), we recover back the solution in the CPU also with a single data transfer. We have executed the same code in the two considered GPU architectures.

The code is implemented as follows. The code is of stencil type, i.e., each node in the grid requires of knowing the values of the variable, whose solution we seek, at a certain number of neighbors as Fig. 1 schematically shows for the cases in which the Laplacian operator is discretized in 9 or 17 points. In the most general case we have implemented, both the central node, identified with the integer indices  $(i, j)$ , where  $1 \leq i \leq N_x$  and  $1 \leq j \leq N_y$  and each of its (at most) 24 neighbors spanned by the discretization of the Laplacian can have different numerical factors weighting their contributions (see, e.g., the values of such coefficients enclosed in the circles shown in Fig. 1, which correspond to the simplest case of a two-dimensional problem in Cartesian coordinates). These numerical factors may change as a function of the position of the central node of the discretization in the grid. We refer to each of these numerical factors with the terminology sketched in Tab. 2. The numerical factor corresponding to the central node at a position  $(i, j)$  is annotated by  $f_C(x_{1,i}, x_{2,j}, \Delta x_{1,i}, \Delta x_{2,j})$ , as it may depend on the general coordinates  $(x_{1,i}, x_{2,j})$  and on the grid spacing between consecutive nodes around the central node  $(\Delta x_{1,i}, \Delta x_{2,j})$ , since we allow for non-uniform meshes. The rest of the numerical factors are named using the cardinal points and numbers (see Tab. 2). To improve the efficiency and to deal more easily with the boundary conditions, in the cases in which the Laplacian is discretized in up to 9 points, we have created a different data structure for this case (upper part of Tab. 2), which we differentiate from the most generic case represented by the lower part of Tab. 2.

As a result of this, the code is totally generic regarding discretization and coordinates: the choice of coordinates determines the discretization of the Laplacian operator, and this discretization determines the mask of the functions (see Table 3). In addition, although the kernels are quite generic, the code allows particular instantiations to the different stencils in a simple and optimal way (without saving repeated values, without operating the zeros, etc.).

Our implementation also takes advantage of memory hierarchy on the

$f_{NW}(x_{1,i}, x_{2,j}, \Delta x_{1,i}, \Delta x_{2,j})$	$f_N(x_{1,i}, x_{2,j}, \Delta x_{1,i}, \Delta x_{2,j})$	$f_{NE}(x_{1,i}, x_{2,j}, \Delta x_{1,i}, \Delta x_{2,j})$
$f_W(x_{1,i}, x_{2,j}, \Delta x_{1,i}, \Delta x_{2,j})$	$f_C(x_{1,i}, x_{2,j}, \Delta x_{1,i}, \Delta x_{2,j})$	$f_E(x_{1,i}, x_{2,j}, \Delta x_{1,i}, \Delta x_{2,j})$
$f_{SW}(x_{1,i}, x_{2,j}, \Delta x_{1,i}, \Delta x_{2,j})$	$f_S(x_{1,i}, x_{2,j}, \Delta x_{1,i}, \Delta x_{2,j})$	$f_{SE}(x_{1,i}, x_{2,j}, \Delta x_{1,i}, \Delta x_{2,j})$

$f_{NW2}$	$f_{NWN}$	$f_{N2}$	$f_{NEN}$	$f_{NE2}$
$f_{NWW}$	$f_{NW}$	$f_N$	$f_{NE}$	$f_{NEE}$
$f_{W2}$	$f_W$	$f_C$	$f_E$	$f_{E2}$
$f_{SWW}$	$f_{SW}$	$f_S$	$f_{SE}$	$f_{SEE}$
$f_{SW2}$	$f_{SWS}$	$f_{S2}$	$f_{SES}$	$f_{SE2}$

**Table 2:** Notation for the functions of neighbors at a distance one and two.

Cartesian coordinates		
0	$\frac{1}{\Delta y^2}$	0
$\frac{1}{\Delta x^2}$	$\frac{-2}{\Delta x^2} + \frac{-2}{\Delta y^2}$	$\frac{1}{\Delta x^2}$
0	$\frac{1}{\Delta y^2}$	0

Polar coordinates		
0	$\frac{1}{r_i^2 \Delta \theta^2}$	0
$\frac{1}{\Delta r_i^2} - \frac{1}{2r_i \Delta r}$	$\frac{-2}{\Delta r^2} + \frac{-2}{r_i^2 \Delta \theta^2}$	$\frac{1}{\Delta r_i^2} + \frac{1}{2r_i \Delta r}$
0	$\frac{1}{r_i^2 \Delta \theta^2}$	0

Bipolar coordinates		
0	$\frac{\cosh \nu_j - \cos \mu_i}{a^2 \Delta \nu^2}$	0
$\frac{\cosh \nu_j - \cos \mu_i}{a^2 \Delta \mu^2}$	$\frac{-2(\cosh \nu_j - \cos \mu_i)}{a^2 \Delta \mu^2} + \frac{-2(\cosh \nu_j - \cos \mu_i)}{a^2 \Delta \nu^2}$	$\frac{\cosh \nu_j - \cos \mu_i}{a^2 \Delta \mu^2}$
0	$\frac{\cosh \nu_j - \cos \mu_i}{a^2 \Delta \nu^2}$	0

**Table 3:** Values of the variables of first table in Table 2 for some specific cases. In all cases we assume uniform meshes. The upper, middle and lower tables correspond to the standard 5-points discretization of the Laplacian operator in Cartesian, polar and bipolar coordinates, respectively.

GPU device, since the kernel uses both the Shared Memory and the Registers on board of the CUDA device. Employing the CUDA Occupancy Calculator (free tool provided by Nvidia), we have tuned a number of parameters of the developed kernel in order to maximize the occupancy of the GPU devices. After some experimentation, we find that a 100% occupancy results employing 256 threads per block and 2048 bytes of shared memory per block independent of the compute capability of the device. The number of registers per thread has been chosen to be 37 (32) for a device with CC = 3.5 (CC = 5.2).

### 3.3. Test problem

We employ a very simple setting to calibrate the new implementation of our algorithm for GPUs. For that we solve a simple Poisson problem with a source term, whose solution is analytically known [4]:

$$\Delta u = -(x^2 + y^2)e^{xy}, \quad (x, y) \in [0, 1]^2, \quad (9)$$

with appropriate Dirichlet boundary conditions. The unit square is discretized in  $N_x \times N_y = 1024 \times 1024$  nodes, where the numerical solution is computed. The boundaries are easily specified in this case, since there exists an analytic solution for the problem at hand, which can be used to compute the boundaries at the edges of the computational domain. The analytic solution reads

$$u(x, y) = -e^{xy}. \quad (10)$$

In next sections, we will take advantage of the knowledge of the analytic solution to compute the reduction of the error with resolution.

### 3.4. Times and ratios

We have solved the test problem of Sec. 3.3, until reaching a prescribed tolerance, using the classical 5-points discretization of the Laplacian, and also the two discretizations of 9-points and 17-points introduced in Sec. 2.1. We employ a resolution dependence tolerance, which decreases as  $N^{-2}$ . For reference, we have solved the problem with the Chebyshev-Jacobi method as well as with the classical Jacobi one. Finally, as we have mentioned before in Sec. 3.1, we have used two different microarchitectures for the implementations which work over GPUs.

Figure 3 shows the computational time (in seconds) as a function of the number of points per dimension  $N$ . For simplicity, we make our measurements in uniform computational meshes satisfying  $N_x = N_y = N$ , so that

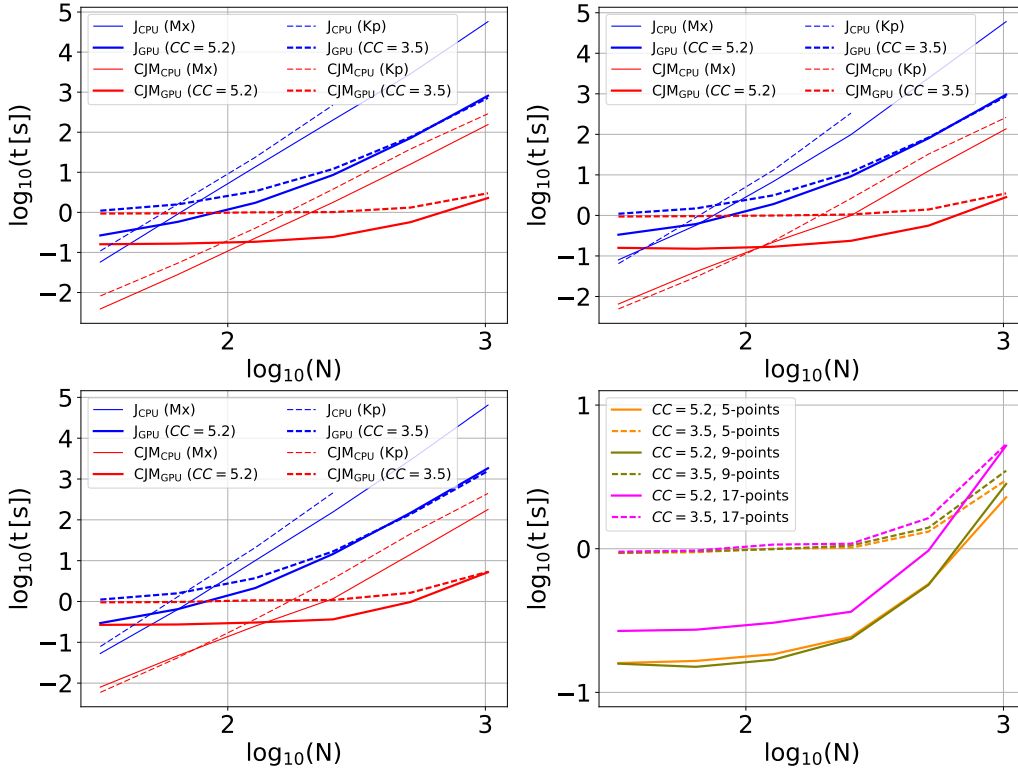


**Figure 3:** Both top and bottom left plots show the time necessary to reach a prescribed tolerance for different methods and implementations. We use a 5-points, 9-points and 17-points stencils in top left, top right and bottom left plots, respectively. Blue (red) lines refer to the Jacobi (Chebyshev-Jacobi) method. Thin (thick) lines correspond to serial code (GPU implementation). Solid (dashed) lines are associated to a Compute Capability equals to 5.2 (3.4). Bottom right plot shows the times of the Chebyshev-Jacobi method over GPUs.

the grid resolution in any of the two spatial directions is  $h = 1/N$ . For low resolutions most of the time in the GPU implementations is consumed by the transfer of data between the host and the device. This time to transfer data is larger than the time required by the method itself. In the different panels of Fig. 3 this effect shows up as a plateau region in the curves corresponding to GPU implementations of, specially, the CJM. The plateau extends up to a certain turnover value  $N_{to}$  (depending on the method and on the architecture of the device), above which we observe that the slopes of the lines stabilize in a very similar way to the one of the sequential execution, but almost two

orders of magnitude below it. For instance, in the upper left panel, of Fig. 3 this flat region extends up to  $N_{\text{to}} \lesssim 300$ . The latency of the data transfers is more obvious in the Kepler architecture (corresponding to a CC of 3.5) than in the case of Maxwell. The turnover in the former device happens at  $N_{\text{to}} \sim 300$  for the CJM run over GPUs, while it is located at  $N_{\text{to}} \sim 256$  for the latter device (see Fig. 3 upper left panel). For the Jacobi method implemented on GPUs, the aforementioned plateau does not exist. The reason for it is twofold. First, the amount of data transfers between the host and the CUDA device is slightly smaller in the latter method. This extra data required by the CJM are the  $M$  weights needed to perform the  $M$  iterations of a complete computational cycle. Second, the Jacobi method is computationally more intensive than the CJM, since the the number of operations per grid node is comparable in both methods, but the number of iterations to reach the tolerance goal is much larger in the Jacobi method than in CJM. As a result, the Jacobi method is relatively more costly with respect to the data transfer. We therefore conclude that a minimum mesh size is needed so that the data transfer time between the CPU and the GPU, and viceversa, is negligible in comparison to the computing time. Furthermore, we note that below certain critical mesh size it is not even advantageous using the CUDA devices, since the CPU implementation of the methods at hand run faster. This is the case, e.g., of the Jacobi method when using the 5-points discretization of the Laplacian displayed in Fig. 3 (upper left panel): where the thin solid (dashed) blue line, corresponding to the CPU executions, exhibit an smaller computational time than the corresponding GPU runs, indicated with thick solid (dashed) lines. Both lines (thin and thick corresponding to the same method) cross at a “critical” value  $N_c \lesssim 64$ . This effect is exacerbated in the test involving the CJM, where the CPU executions are faster than the corresponding GPU ones for  $N_c \lesssim 128$ . Noteworthy, comparing the upper left panel of Fig. 3 with the upper right and bottom left panels of the same figure, the effectiveness of the GPU implementation of the CJM over the corresponding CPU does not depend on the stencil of the discretization of the Laplacian.

From the bottom right plot, where only the Chebyshev-Jacobi method on GPUs is plotted, we observe that the qualitative behavior is quite similar for all the different stencils. Comparing results obtained in the two CUDA devices with the same discretization of the Laplacian, it is evident that the architecture of Maxwell (CC = 5.2) is faster than that of Kepler. However, the gap between both architectures reduces as the resolution increases. Actu-

ally, the difference in execution time between both devices displays a trend to reduce as the number of points in the discretization of the Laplacian grows, particularly beyond the value of  $N_{to}$  for each test. This is remarkably visible for the 17-points discretization of the Laplacian (pink lines of Fig. 3 bottom right panel), since at the highest resolution of our tests ( $N = 1024$ ), the computational time is the same in both devices. This happens in spite of the fact that Maxwell architecture is faster regarding both transfers and executions. However, Kepler architecture is better suited for double precision computations, which we employ in practical applications of the elliptic solver at hand.

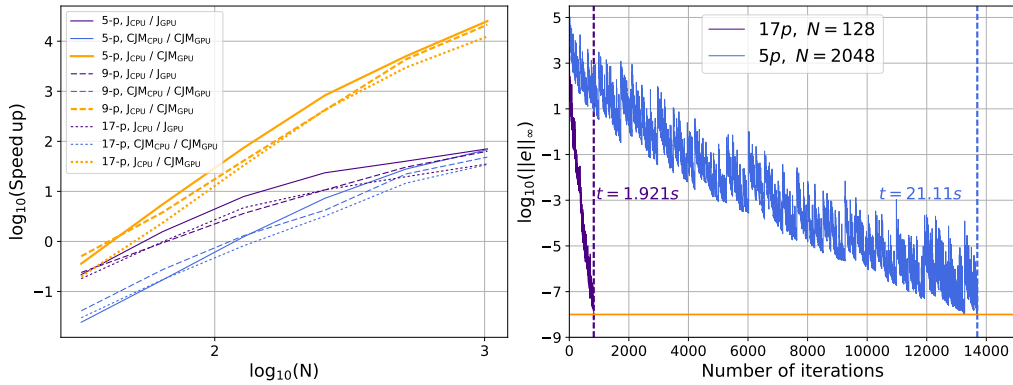


**Figure 4:** Left: Ratio of computational time in a CPU execution to the computational time in an analogous GPU execution as a function of the number of points per dimension. Solid lines correspond to the 5-points stencil, dashed lines to the 9-points stencil and dotted lines to the 17-points stencil. Blue and purple lines represent the ratios between the times of the sequential versus the parallel implementations of the Jacobi and Chebyshev-Jacobi methods. Orange lines represent the ratio between the time of the slowest method, the sequential implementation of the Jacobi method, and the fastest one, the Chebyshev-Jacobi method in parallel over GPUs. Right: Real error versus number of iterations for a 17-points stencil with a mesh of  $N = 128$  points (purple line) and a classical 5-points stencil with a mesh of  $N = 2048$  points (blue line), until reaching a real error of  $10^{-8}$  (orange horizontal line). The vertical dashed lines indicate the final number of iterations. The computational times of each run are also labeled in the plot.

In Figure 4 we plot the ratios between the times of different methods and implementations. These ratios provide an estimation of the acceleration factor by which the GPU implementation of either the CJM or the Jacobi

method is faster (or slower) than any other of the methods. The figure also displays the dependence of the speed up of the GPU versions on the three types of stencil. We observe that the larger number of points the stencil has, the smaller is the speed up. The improvement over the CPU implementation is larger for the Jacobi method than for the CJM (note that the purple solid line lies above any of the blue lines in left panel of Fig. 4). However, this larger relative speed up in the Jacobi method, with the smallest number of discretization points of the Laplacian, reduces with either increasing values of  $N$ , or when considering higher-order discretizations of the Laplacian. In the latter case, the speed up of the CJM over GPUs equals that of the corresponding Jacobi method employing a 17-points discretization of the Laplacian when  $N = 1024$ . In fact, extrapolating the results to even higher resolutions (not included in the plot) we foresee that the speed up factor of the CJM over its corresponding sequential CPU implementation will be better than that of the Jacobi method. From the ratio between the CJM on GPUs, and the slowest one, the classical Jacobi method in sequential, it can be appreciated the difference of several orders of magnitude in the speed up for high resolutions (see orange lines in left panel of Fig. 4).

In addition to Fig. 4, we list the values of the ratios for the particular case of a mesh with  $N = 1024$  points per dimension in Table 4. In this table we systematically include the speed up factors of each of the methods listed in the columns with respect to the methods annotated in the rows in which the stencil of the Laplacian discretization is provided.

Finally, as we have already shown in [4], it proves convenient to use a higher order discretization of the operator although it involves larger stencils. In the latter case the computational time due to the fact of having more points to get a solution of the same quality is negligible compared to the reduction in time due to the smaller number of iterations needed. To illustrate this point, we use the CJM on GPUs (our method of choice). We understand that having solutions of the same quality means reaching the same "real" error level. By real error we denote the difference, in infinity norm, between the obtained numerical solution and the analytical one. Since we have the analytical solution (10) of the the test problem (9), we can use the real error instead of a tolerance as the stopping criterion. In Fig. 4 we plot the real error versus number of iterations using, on one hand, a 17-points stencil with a mesh of  $N = 128$  points and, on the other hand, a classical 5-points stencil with a mesh of  $N = 2048$  points, until reaching a prescribed value of the real error ( $10^{-8}$ ); in addition to the smaller resolution needed for the higher order

<b>5-points</b>	j	j_GPU	cj	cj_GPU
j	1	–	–	–
j_GPU	71	1	–	–
cj	371	5	1	–
cj_GPU	25235	357	68	1
<b>9-points</b>	j	j_GPU	cj	cj_GPU
j	1	–	–	–
j_GPU	63	1	–	–
cj	441	7	1	–
cj_GPU	21360	337	48	1
<b>17-points</b>	j	j_GPU	cj	cj_GPU
j	1	–	–	–
j_GPU	35	1	–	–
cj	361	10	1	–
cj_GPU	12420	352	34	1

**Table 4:** Speed up factors of each of the methods listed in the columns with respect to the methods annotated in the rows in which the stencil of the Laplacian discretization is provided. All the values correspond to the test problem of Sec. 3.3 evaluated on a grid with  $N = 1024$  points per dimension.

method (17-points stencil), we have a reduction of one order of magnitude both in the number of iterations and in the computational time.

#### 4. Conclusions

In previous papers [3, 4], we have delineated the potential degree of parallelism of the CJM method as a major advantage over other competing algorithms to solve linear systems of equations resulting from the discretization of elliptic systems of partial differential equations. Building upon the basic Jacobi method, the parallel implementation of the CJM is as simple as that of the former method. Here we have materialized our previous claims and presented a GPU based implementation of the CJM. We have tested the CUDA ported Jacobi and CJ algorithms in two different GPU architectures with compute capabilities of 3.5 and 5.2. Even though the Maxwell architecture (with compute capability 5.2) is more recent and potentially faster than the Kepler one (with  $CC = 3.5$ ), the differences in actual computing time reduce significantly as either the grid size increases or the number of points employed in the discretization of the Laplacian grows. We find that it is possible to speed up by several orders of magnitude the classical Jacobi method thanks to the use of the parallel implementation of the CJM on GPUs.

Moreover, we have illustrated the benefits from using the parallel implementation of the CJM over GPUs in combination with a high-order discretization of the Laplacian operator in a test problem. We conclude that it is always advantageous employing high-order discretizations of the elliptic operator since they require less iterations and less computational time to reach the same real error goal. This conclusion is independent of the parallel implementation of any of the methods we have tested in this paper. However, the combination of high-order discretization of the elliptic operators and the CJM implemented on GPUs results in an extremely powerful method for practical applications.

#### Acknowledgments

We thank Marc Jordà from the Barcelona Supercomputing Center for his contribution in the implementations using GPUs. We acknowledge the support of the Consolider SyeC net TIN2014-52608-REDC. We also acknowledge the support from the European Research Council (Starting Independent Researcher Grant CAMAP-259276) and from the Spanish Ministerio

de Economía y Competitividad through the grants SAF2013-49284-EXP, AYA2015-66899-C2-1-P, as well as the support of the Valencia Government through the grant PROMETEO-II-2014-069.

## References

- [1] X. I. Yang, R. Mittal, Acceleration of the jacobi iterative method by factors exceeding 100 using scheduled relaxation, *Journal of Computational Physics* 274 (2014) 695 – 708. doi:<http://dx.doi.org/10.1016/j.jcp.2014.06.010>.  
URL <http://www.sciencedirect.com/science/article/pii/S0021999114004173>
- [2] J. E. Adsuara, I. Cordero-Carrión, P. Cerdá-Durán, M. A. Aloy, Improvements in the Scheduled Relaxation Jacobi method, in: C. Díaz Moreno, J. M. and Díaz Moreno, J. C. and García Vázquez, C. and Medina Moreno, J. and Ortegón Gallego, F. Pérez Martínez, M. V. Redondo Neble, J. R. Rodríguez Galván (Eds.), *Proceedings of the XXIV Congress on Differential Equations and Applications / XIV Congress on Applied Mathematics* Cádiz, June 8-12, 2015., Servicio de Publicaciones de la Universidad de Cádiz, 2015.
- [3] J. Adsuara, I. Cordero-Carrión, P. Cerdá-Durán, M. Aloy, Scheduled relaxation jacobi method: Improvements and applications, *Journal of Computational Physics* 321 (2016) 369 – 413. doi:<http://dx.doi.org/10.1016/j.jcp.2016.05.053>.  
URL <http://www.sciencedirect.com/science/article/pii/S002199911630198X>
- [4] J. Adsuara, I. Cordero-Carrión, P. Cerdá-Durán, V. Mewes, M. Aloy, On the equivalence between the scheduled relaxation jacobi method and richardson's non-stationary method, *Journal of Computational Physics* 332 (2017) 446 – 460. doi:<http://dx.doi.org/10.1016/j.jcp.2016.12.020>.  
URL <http://www.sciencedirect.com/science/article/pii/S0021999116306738>
- [5] L. M. Adams, R.-J. LeVeque, D. Young, Analysis of the sor iteration for the 9-point laplacian, *SIAM Journal on Numerical Analysis* 25 (5) (1988)

1156–1180. doi:10.1137/0725066.  
URL <http://dx.doi.org/10.1137/0725066>

- [6] Cuda.  
URL [http://www.nvidia.com/object/cuda\\_home\\_new.html](http://www.nvidia.com/object/cuda_home_new.html)